ESC European Society of Cardiology

Cardiovascular Research (2020) **116**, 1525–1538
doi:10.1093/cvr/cvz238

Endothelial microvesicles carrying Src-rich cargo impair adherens junction integrity and cytoskeleton homeostasis

Victor Chatterjee[1], Xiaoyuan Yang[1], Yonggang Ma [1], Byeong Cha [1], Jamie E. Meegan [1], Mack Wu[2], and Sarah Y. Yuan[1,2]*

[1]Department of Molecular Pharmacology and Physiology, University of South Florida Morsani College of Medicine, Tampa, FL 33612, USA; and [2]Department of Surgery, University of South Florida Morsani College of Medicine, Tampa, FL 33612, USA

Received 1 April 2019; revised 6 August 2019; editorial decision 23 August 2019; accepted 29 August 2019; online publish-ahead-of-print 3 September 2019

Time for primary review: 15 days

Aims Microvesicles (MVs) conduct intercellular communication and impact diverse biological processes by transferring bioactive cargos to other cells. We investigated whether and how endothelial production of MVs contribute to vascular dysfunction during inflammation.

Methods and results We measured the levels and molecular properties of endothelial-derived MVs (EC-MVs) from mouse plasma following a septic injury elicited by cecal ligation and puncture, as well as those from supernatants of cultured endothelial cells stimulated by inflammatory agents including cytokines, thrombin, and complement 5a. The mouse studies showed that sepsis caused a significant increase in total plasma vesicles and VE-cadherin$^+$ EC-MVs compared to sham control. In cultured ECs, different inflammatory agents caused diverse patterns of EC-MV production and cargo contents. When topically applied to endothelial cells, EC-MVs induced a cytoskeleton-junction response characterized by myosin light chain phosphorylation, contractile fibre reorganization, VE-cadherin phosphorylation, and adherens junction dissociation, functionally measured as increased albumin transendothelial flux and decreased barrier resistance. The endothelial response was coupled with protein tyrosine phosphorylation promoted by MV cargo containing c-Src kinase, whereas MVs produced from c-Src deficient cells did not exert barrier-disrupting effects. Additionally, EC-MVs contribute to endothelial inflammatory injury by promoting neutrophil-endothelium adhesion and release of neutrophil extracellular traps containing citrullinated histones and myeloperoxidase, a response unaltered by c-Src knockdown.

Conclusion Endothelial-derived microparticles cause endothelial barrier dysfunction by impairing adherens junctions and activating neutrophils. The signalling mechanisms underlying the endothelial cytoskeleton-junction response to EC-MVs involve protein phosphorylation promoted by MV cargo carrying c-Src. However, EC-MV-induced neutrophil activation was not dependent on c-Src.

Keywords Microvesicles • Endothelial cells • Neutrophils • Inflammation • Barrier function

1. Introduction

The vascular endothelium forms a barrier to control the permeability of fluids, proteins, and blood cells. Disruption of this barrier leads to plasma leakage and neutrophil infiltration, a pathological process underlying inflammatory response to sepsis and tissue injury.[1–3] In addition to barrier function, the healthy endothelium maintains circulatory homeostasis by regulating local perfusion and controlling platelet and neutrophil activity. During inflammation, a heterogeneous population of vesicles, called microvesicles (MVs), are produced by activated endothelial cells and released into the circulation.[4] These MVs, ranging from 0.1 μm to 1 μm in diameter, serve as important vehicles of intercellular communication

* Corresponding author. Tel: +1 813 974 5104; fax: 813-974-3079, E-mail: syuan@health.usf.edu

through transferring diverse cargos from parent cells to target cells in regulating multiple biological processes.[5] The production and molecular composition of circulating MVs of endothelial origin (EC-MV) are altered in cardiovascular diseases such as acute coronary syndromes, hypertension, diabetes, atherosclerosis, and pre-eclampsia.[6–9] Their significance as potential diagnostic biomarkers in predicting clinical outcomes has been highlighted.[10,11]

EC-MVs in the circulation not only indicate the pathophysiological state of their parent endothelium, but also contribute to disease pathogenesis via interactions with other blood components and vascular tissues distal to the site of inflammation. For example, EC-MV-platelet aggregates are increased in stable coronary artery disease,[12] and EC-MV-monocyte aggregates are increased in venous thromboembosis.[13] Circulating MVs from pre-eclampsia and myocardial infarction patients, as well as endothelial MVs generated *in vitro*, have been shown to impair endothelium-dependent vasorelaxation.[14–17] While many studies have focused on the pro-coagulant and pro-inflammatory nature of circulating MVs, their role in regulating endothelial barrier function has not been well-studied. In particular, it is not clear how EC-MVs interact with target endothelial cells and how such interactions affect endothelial cytoskeleton organization or junction permeability.

Recent studies have shown altered MV production in the circulation during systemic inflammatory responses to injury or sepsis.[18] Since inflammation is associated with increased levels of cytokines,[19,20] complements,[21,22] and thrombin,[23] it is plausible that these agents contribute to MV generation. To date, cell-specific mechanisms of MV generation in response to specific inflammatory agents and their effects on endothelial barrier property remain poorly understood. In this study, we tested the hypothesis that EC-MVs released from activated endothelial cells contribute to vascular inflammatory injury directly by disrupting endothelial cytoskeleton-junction homeostasis and indirectly by activating neutrophils. Given the importance of vascular endothelium as both causal factor and effector of inflammatory injury, we focused on the endothelial effects of EC-MVs. We examined the generation and phenotypes of EC-MVs *in vivo* using a clinically relevant mouse model of sepsis (cecal ligation and puncture, CLP), as well as *in vitro* using cultured human umbilical vein endothelial cell (HUVEC) monolayers stimulated with typical inflammatory agents.

2. Methods

2.1 Antibodies and reagents

Annexin V (Cat # 640918) and Annexin V staining buffer (Cat # 422201), CFSE cell division kit (Cat # 423801), human recombinant TNFα (Cat # 570104), IL-1β (Cat # 592104), IL-6 (Cat # 570804), IFN-γ (Cat # 570204), flow cytometry antibodies against human or mouse CD11b (Cat # 101226), CD66b (Cat # 305104), PECAM-1 (Cat # 303120), ICAM-1 (Cat # 353108), VCAM-1 (Cat # 305806), EPCR (Cat # 351906), VE-Cadherin (Cat # 138016), endoglin (Cat # 323206), E-Selectin (Cat # 336012), mouse IgG_{2a} (Cat # 400212), and IgG_3 isotype control (Cat # 401301) were from Biolegend (San Diego, CA, USA). Alexa Fluor 488 Cav-1 (Cat # sc-53564), Alexa Fluor 647 NOSIII (Cat # sc-376751), c-Src (Cat # sc-5266), ICAM-1 (Cat # sc-390483), VE-Cadherin (sc-9989), GAPDH (Cat # sc-365062), Tyr^{416} phospho-c-Src (Cat # sc81521), control siRNA (Cat # sc-37007), and c-Src siRNA (Cat # sc-29228) were from Santa Cruz Biotechnology, Inc. (Dallas, TX, USA). Antibodies to beta-catenin (Cat # 2677S), phospho-tyrosine (Cat # 8954S), and pMLC2 (Thr18/Ser19) (Cat # 3674) were from Cell Signaling Technologies (Danver, MA, USA). Megamix Plus SSC (Cat # 7803) and MP count beads (Cat # 7804) were from Biocytex (Marseille, France). UltraComp eBeads™ (Cat # 01-2222-41), SYTOX™ Green Nucleic Acid Stain (Cat # S7020), exosome depleted FBS (Cat # A2720803), Alexa Fluor secondary antibodies and phalloidin (Cat #s A31573, A10042, A31571, A10037, A12380, and A22287) were from Thermo Fisher Scientific (Waltham, MA, USA). Anti-cortactin (Cat # 05-180), MLC2 antibody (Cat # MABT180), and Histopaque (Cat # 1077-1/1191-1) were from Millipore Sigma (Burlington, MA, USA). Anti-Citrullinated Histone 3 antibody (Cat # ab5103) and anti-myeloperoxidase antibody (Cat # ab9535) were from Abcam (Cambridge, MA, USA). Thrombin (Cat # 9002-04-4) and PP1 (Cat # 14244) were from Cayman Chemical (Ann Arbor, MI, USA). Human recombinant C5a (Cat # 2037-C5-025) was from R&D Systems (Minneapolis, MN, USA). Blocking buffer (Cat # 927-50000), IRDye secondary antibodies for western blot (Cat # 926-32212, 32213, 68073), and beta-actin antibody (Cat # 926-42212) were from Licor Biosciences (Lincoln, NE, USA). HUVECs from pooled donors (Cat # C-12203) and EGM2 media (Cat # C-22011) were from PromoCell (PromoCell GmbH, Heidelberg, Germany). RPMI media (Cat # 30-2001™) was from ATCC (Manassas, VA, USA).

2.2 Animal studies

All animal studies were approved by the University of South Florida Institutional Animal Care and Use Committee and were performed in accordance with the NIH Guide for the Care and Use of Laboratory Animals (NIH Publication 8th edition, Washington (DC): National Academies Press (US); 2011). C57BL/6 mice (Jackson laboratory) of both sexes, age 12–16 weeks, weighing between 20 and 30 g were used in our studies. Mice were maintained under a 12/12-h light/dark cycle with food and water *ad libitum*. CLP was performed to induce polymicrobial sepsis, as previously described.[24] In brief, the cecum was exposed from anaesthetized mice (100 mg/kg ketamine, i.p. and 10 mg/kg xylazine, i.p.), tightly ligated at 5 mm below the ileocecal valve and perforated twice with a 20-gauge needle distal to the point of ligation. One millimetre of faecal matter was extruded from each puncture hole. The cecum was then repositioned inside the abdomen, and the abdominal cavity was closed in two layers. Body temperature was maintained at 37°C during the surgical procedure by a heating pad. Mice then received Ringers's lactate solution for resuscitation and sustained release buprenorphine (1 mg/kg s.c.) for analgesia. Sham controls were subjected to the same surgical procedures without ligation and puncture. Blood was collected by cheek puncture from sham and CLP mice after 24 h and euthanized by cervical dislocation. Mouse blood was centrifuged at 250 *g* for 30 min without brake at room temperature (RT), followed by centrifugation at 2500 *g* for 30 min at RT to generate platelet poor plasma. Platelet poor plasma was centrifuged at 12 000 *g* for 2 min at 4°C to remove any residual platelets, and platelet free plasma (PFP) was collected and stored at -80°C till further use.

2.3 Human blood collection

Human blood collection was done according to the University of South Florida IRB approved protocol (#19649) and conforming to the principles outlined in the Declaration of Helsinki. After obtaining informed consent, 30 mL of blood was obtained from healthy adult volunteers of either sex between the ages of 18 and 56 years. Peripheral venous blood was collected in BD vacutainer tubes (Cat # 367880) containing 158

USP units of Lithium Heparin and was immediately transferred to the laboratory with minimal agitation.

2.4 Cell experiments

Polymorphonuclear leucocytes (PMNs or neutrophils) were isolated using a double gradient of histopaque 1077 and 1191. Isolated PMNs were seeded on 96 well plates or coverslips in RPMI media +10% foetal bovine serum (FBS). HUVECs of passage 3–5 were seeded in 0.1% gelatin-coated plates and fed by EGM2 media supplemented with growth supplement mix. Cells were incubated in 5% CO_2 humidified incubator at 37°C for use in experimental assays.

2.5 Collection of MVs from EC culture supernatant

HUVECs were grown to confluence in complete EGM2 media in six well plates, washed three times with HBSS and then cultured in serum free EGM2 media with various inflammatory mediators (100 ng/mL TNFα, 100 ng/mL IFNγ, 100 ng/mL IL-1β, 100 ng/mL IL-6, 10 nM C5a, or 10 U/mL thrombin) for 16 h. The supernatant was collected and centrifuged at 300 *g* for 15 min to remove dead cells, followed by centrifugation at 2500 *g* for 30 min at 4°C to remove cell debris and apoptotic bodies. The cell free supernatant was centrifuged at 20 000 *g* for 90 min at 4°C to collect the MV pellet. For functional studies, where MVs were added to cells, the MV pellet was washed with 0.1 μm filtered PBS twice and centrifuged at 20 000 *g* for 90 min to get the final MV pellet that was reconstituted in 100 μL of 0.1 μm filtered PBS and stored at -80°C till further use.

2.6 Transmission electron microscopy

The MV pellet from mouse plasma was fixed with 2% paraformaldehyde for 30 min. MV suspension (5 μL) was loaded on to formvar coated 200 mesh copper EM grids, stained with 1% uranyl acetate, washed, dried, and observed under a transmission electron microscope (JEOL1400, Tokyo, Japan).

2.7 Nanoparticle tracking analysis

Size and concentration of extracellular vesicles (EVs) were measured by the NanosightNS300 (Malvern, Amesbury, UK). In brief, 10 μL of mouse PFP were diluted with 0.39 mL of 0.1 μm filtered PBS and loaded into the sample chamber of the NS300 unit by a syringe pump. Five videos of 60 s were recorded for each sample. Data analysis was performed with the NTA 3.2 software (Nanosight).

2.8 Multi-colour flow cytometry

Twenty microlitre of mouse PFP in 80 μL of FACS buffer was stained with anti-mouse VE-cadherin antibodies (1:100 dilution) for 30 min at RT. Twenty microlitre of EC-MV suspension in 80 μL of FACS buffer was stained with Annexin V, antibodies against human ICAM-1, VCAM-1, E-selectin, PECAM-1, Cav-1, eNOS, endoglin, EPCR, and c-Src (1:100 dilution for all antibodies) for 30 min at RT. Twenty microlitre of MV count beads (size 3 μm) and 300 μL of Annexin V binding buffer or FACS buffer was added to the sample, flow cytometry was performed on BD^{TM} LSRII, and the data were analysed by BD FACS Diva^{TM} software, v6. Side-scatter based MV size gate (corresponding to MV size range of 0.1–1 μm) was done with the assistance of 0.5, 0.24, 0.20, and 0.16 μm sizing beads, and all events were recorded with a forward scatter threshold of 200 according to the company's instructions. The size gate excluded exosomes less than 0.1 μm and apoptotic bodies or cell debris larger than 1 μm in size. The final MV count was calculated by the following formula: Actual MV count = [(number of MV counted × MV count bead concentration)/number of MV count beads counted] according to the company instructions. The log height signal was used to quantify MVs.

Whole blood (WB) was treated with EC-MVs (1×10^6) or PBS for 2 h at RT. Treated WB was stained with anti-CD66b (1:100) and CD11b (1:100) in 100 μL of FACS buffer for 30 min at RT, fixed with 1% PFA, followed by multi-colour FCM using BD^{TM} LSRII to study PMN activation. Data analysis was done by Flow Jo v10.5.

HUVECs were treated with EC-MVs for 4 h. Live cells were stained with anti-human ICAM-1 (1:100) and VCAM-1 (1:100) for 30 min on ice. Flow cytometry was performed on BD^{TM} LSRII, and the data analysed by Flow Jo v10.5.

2.9 Immunofluorescence

HUVECs were grown to confluence on 0.1% gelatin-coated coverslips. MVs were stained with 5 μM carboxyfluorescein succinimidyl ester (CFSE), washed twice, and added to a confluent HUVEC monolayer. After 8 h, cells were washed with PBS to remove non-adherent MVs. Cells were then fixed with 4% PFA for 15 min at RT, washed, blocked with PBS + 2% BSA + 0.1% Triton X for 30 min followed by incubation with anti-human phospho-tyrosine, cortactin, pMLC2 (Thr18/Ser19), VE-Cadherin, beta-catenin, Tyr^{658} phospho-VE-Cadherin, ICAM-1, and CD11b antibodies in blocking buffer (1:100) overnight at 4°C. Coverslips were then washed twice with PBS + 0.1% Triton X and incubated with fluorescently conjugated appropriate secondary antibodies (1:200) for 1 h at RT. F-actin staining was performed using Alexa Fluor conjugated phalloidin during secondary antibody incubation. Coverslips were washed, dried, mounted on glass slides with ProLong^{TM} diamond antifade mountant containing DAPI, and imaged by an Olympus FV1200 or Leica SP8 Spectral Inverted Laser Scanning Confocal Microscope. Integrated density (area X mean fluorescence intensity) from all sections of an entire confocal z stack was collected and quantitatively analysed using Image J V2.0.0.

In some experiments, PMNs were treated with CFSE stained EC-MVs for 2 h to study their interactions with EC-MVs. Coverslips were fixed, blocked, washed, and probed as mentioned above. Coverslips with PMNs were stained with myeloperoxidase (MPO) and anti-citrullinated histone 3 (1:100) overnight at 4°C followed by Alexa Fluor conjugated secondary antibodies (1:200) to study NETosis after EC-MV interaction. All coverslips were mounted onto glass slides with ProLong^{TM} diamond antifade mountant containing DAPI for imaging under 63× oil objective with a 4.0× optical zoom by an Olympus FV1200 Spectral Inverted Laser Scanning Confocal Microscope.

2.10 Endothelial monolayer permeability to albumin

HUVECs (2×10^4) were seeded on Corning Co-Star transwell membrane (pore size 0.4 μm). Twenty microlitres (~1×10^6) EC-MV or buffer was added to the cells at an MV:HUVEC ratio of approximately 50:1),[25] followed by 1 mg/mL of fluorescein isothiocyanate (FITC) conjugated albumin (Cat. # A-9771, Sigma Aldrich) for 9 or 16 h, and albumin transendothelial flux was measured using a fluorescence microplate reader (Molecular Devices, San Jose, CA, USA). The permeability coefficient of albumin (*Pa*) was calculated as $Pa = [Ab]/t \times 1/A \times V/[L]$, where [Ab] is the bottom chamber (ablumenal) concentration, *t* is the time (s),

A is the area of the membrane (cm^2), V is the bottom chamber volume, and [L] is the top chamber (lumenal) concentration.

2.11 SiRNA transfection

Transfections of siRNA against c-Src were conducted using 4D-Nucleofector™ systems (Lonza, Switzerland). HUVECs were trypsinized, washed, pelleted, and resuspended with 100 µL of P5 primary cell 4D-Nucleofector™ solution containing 1 µM c-Src siRNA or scrambled siRNA. After electroporation was done using CA-167 programme, ECs were plated onto 0.1% gelatin-coated culture dishes and cultured for 48 h. Transfected cells were then treated with 100 ng/mL TNFα for 16 h, and EC-MVs collected from supernatant as described above.

2.12 Western blot analysis

HUVECs were grown in six well plates and treated with EC-MV (MV:HUVEC ratio ∼50:1) or buffer for 8 h. In some experiments, HUVECs were treated with scrambled or c-Src knockdown EC-MVs. Cells were then lysed in 1× RIPA lysis buffer containing protease and phosphatase inhibitors. Protein quantitation was performed by BCA assay and reduced cell lysates run on a 4–20% Tris-Glycine gel and transferred onto a nitrocellulose membrane. Membrane was blocked in Licor blocking buffer for 1 h at RT, probed with primary antibodies in blocking buffer + 0.1%Tween 20 (1:1000) overnight at 4°C, washed with 1 × TBS + 0.1% Tween 20 thrice for 10 min, and probed with Licor IRDye secondary antibodies in blocking buffer + 0.1%Tween 20 + 0.05% SDS (1:20 000) for 1 h at RT. The washed membranes were then imaged on Licor Odyssey CLx and blots were quantitated by using the Image Studio Lite, v 5.2.5.

2.13 PMN-EC adhesion assay

HUVECs were grown to confluence in clear bottom 96 well plates. Cells were treated with EC-MVs for 4 h and washed with PBS three times to remove all non-adherent MVs. PMNs were stained with 1 µM Calcein AM in serum free RPMI media for 30 min at 37°C, washed twice with PBS and then re-suspended in complete RPMI. Labelled PMN (1×10^4) were added to each well and incubated for 1 h at 37°C and 5% CO_2. The wells were then washed thrice with PBS to remove any non-adherent neutrophils. A 200 µL of PBS was added to each well and the number of adherent PMN analysed by fluorescence intensity recorded by a spectrophotometer.

2.14 Sytox green assay measuring NETs

Neutrophil suspension (1×10^5) in RPMI media + 10% FBS were seeded in black clear bottom 96 well plates (Costar) and allowed to settle for 30 min in an incubator at 37°C and 5% CO_2. Twenty microlitres of buffer or EC-MV (1×10^6) were added to PMNs and incubated for 2 h. Sytox green (final concentration 1 µM) was added to each well and incubated at 37°C for 15 min. Fluorescence was recorded by a spectrophotometer at excitation 500 nm and emission 525 nm. In some wells, DNAase 1 and Triton X were added 30 min before addition of Sytox green. Percentage of NETosis was calculated as:

$$[(\text{PMN} + \text{Buffer/EC-MV}) - (\text{PMN} + \text{Buffer/EC-MV} + \text{DNAase-1})] / (\text{PMN} + \text{Triton-X}) \times 100.$$

2.15 Statistical analysis

All data are expressed as mean ± SEM. All data meet normal distribution assumption. Multiple comparisons were performed by one-way ANOVA with Dunnett's or Tukey's multiple comparison tests (GraphPad Prism 7). Comparisons between two groups were performed using an unpaired Student's *t*-test. A *P*-value <0.05 was considered to be significant.

3. Results

3.1 Sepsis increases EC-MV production

We first tested whether septic injury affects endothelial production of EVs including exosomes (30–100 nm) and MVs (100–1000 nm). CLP was performed to induce sepsis. The number and size of plasma total EVs were evaluated by nanoparticle tracking analysis (NTA) 24 h after CLP (*Figure 1A*). The results showed that plasma from septic mice contained a significant higher number of total EVs, compared to sham control (*Figure 1A(i–iii)* and *B*). The majority of EVs were between 100 and 200 nm in size as seen by NTA measurements and TEM (*Figure 1A* and *C*). MV quantitation and phenotypic characterization using cell-specific markers were performed by multicolour flow cytometry using 0.1–1µm MV sizing beads and MV count beads. In line with EV data shown above, septic mouse plasma had significantly increased levels of total MVs (*Figure 1D*) and VE-cadherin$^+$ EC-MVs (*Figure 1E* and *F*).

3.2 *In vitro* inflammatory stimulation alters endothelial MV numbers and cargo

We examined the quantity and molecular characteristics of MVs generated from endothelial cells during stimulation by different pro-inflammatory agents that are known to increase in the circulation during sepsis, including TNFα, IFNγ, IL-1β, IL-6, C5a, or thrombin. We investigated which inflammatory stimuli induced the maximum production of MVs that express markers of cell injury or activation, such as phosphaditylserine (PS), intercellular adhesion molecule 1 (ICAM-1), vascular adhesion molecule 1 (VCAM-1), endothelial selectin (E-selectin), and platelet endothelial cell adhesion molecule 1 (PECAM-1). *Figure 2A* shows that TNFα was the most potent among the other pro-inflammatory agents, as it caused a significant increase in PS$^+$, ICAM-1$^+$, VCAM-1$^+$, PECAM-1$^+$, and E-selectin$^+$ MVs. Quantification analyses (*Figure 2B* and *C*) demonstrate that TNFα induced a greater number of EC-MVs that express all of the above injury/activation markers, whereas IL-1β only caused a significant increase in E-selectin$^+$ EC-MVs (*Figure 2C*). Since TNFα demonstrated a most potent effect among all inflammatory agonists tested, we used TNFα as the primary stimulus for generating EC-MVs for the rest of our study. We further found that EC-MVs released from unstimulated HUVECs expressed endothelial protein C receptor (EPCR) on their surface which was reduced in TNFα-induced EC-MVs (*Figure 2D* and *E*). TNFα treated endothelial cells also displayed significantly increased production of MVs that were endoglin$^+$, caveolin-1 (Cav-1)$^+$, and endothelial nitric oxide (eNOS)$^+$, however, eNOS expression on MVs was significantly reduced after TNFα treatment (*Figure 2D–F*).

3.3 EC-MVs increase albumin permeability by disrupting junction integrity

We investigated whether EC-MVs can induce barrier dysfunction when added to endothelial monolayers *in vitro*. *Figure 3A–D* shows that EC-MVs interacting with HUVECs caused disruption of VE-cadherin/beta-catenin complexes at cell–cell junctions. Consistent with the notion that disruption of adherens junctions leads to an increased endothelial

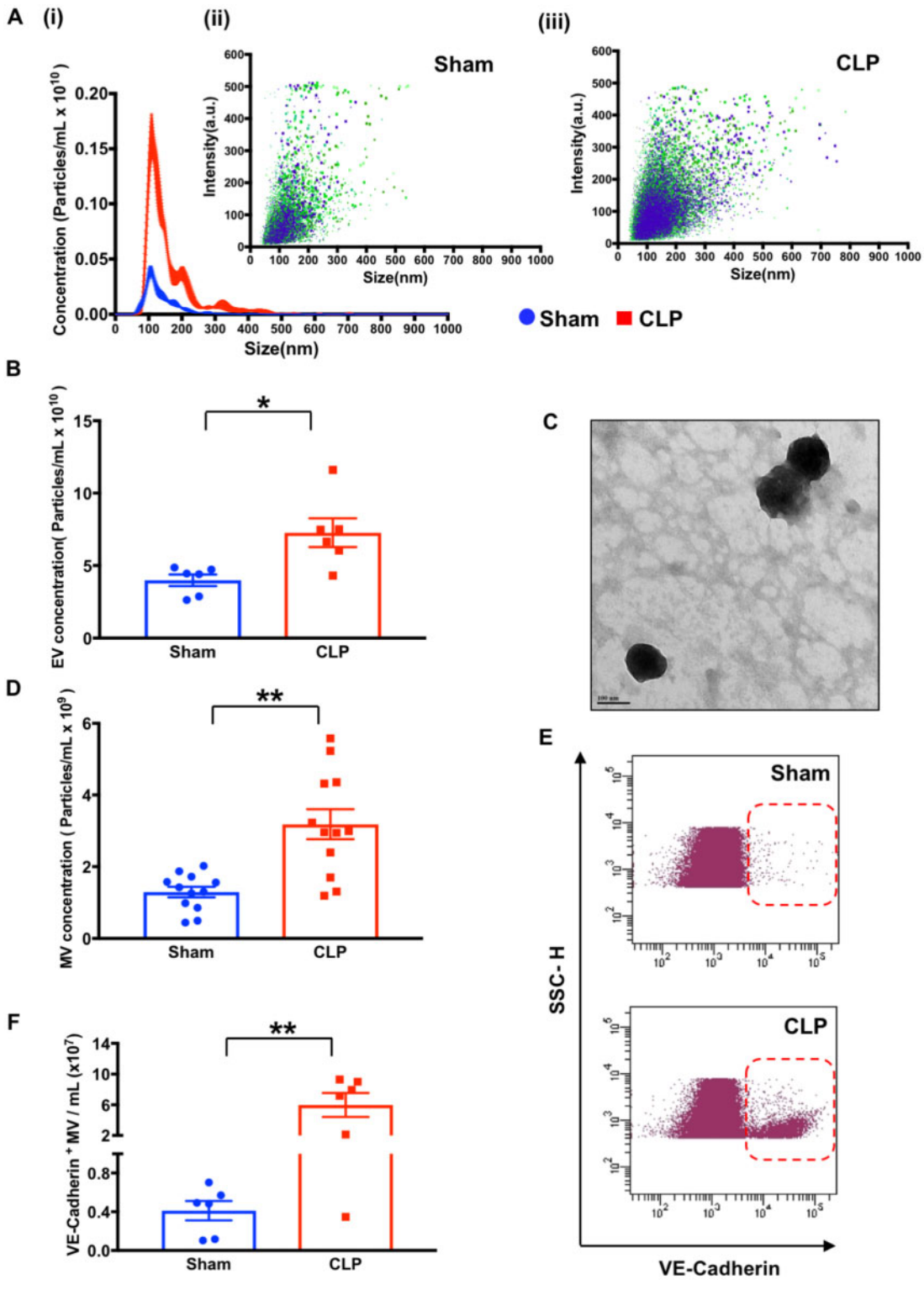

Figure 1 EV levels are increased in mouse plasma during CLP-induced sepsis. (*A*) Representative NTA tracings show increased concentration of EVs in septic plasma as compared to sham. (i) Merged concentration-size plots of EVs from sham and CLP plasma. The red (CLP) and blue (sham) line graphs show individual concentration values plotted against particle sizes derived from five separate NTA readings. (ii and iii) Intensity-size plots of EVs from mouse plasma that underwent sham surgery or CLP, respectively showing increased particles in CLP plasma. The different shades of green and blue scatter points represent particle tracings from five separate readings. (*B*) Quantification of NTA analyses shows that the total EV numbers are significantly increased in CLP plasma compared to sham plasma. (*C*) TEM image of plasma MVs showing particles near the 100 nm size range. Scale bar = 100 nm. Flow cytometry analyses show significantly increased total MV numbers (*D*) and VE-Cadherin^{+} MVs in the plasma of CLP mice (*E* and *F*). All data are presented as mean ± SEM. *$P < 0.05$, **$P < 0.01$ between sham and CLP by Student's *t*-test, $n = 6–12$ animals.

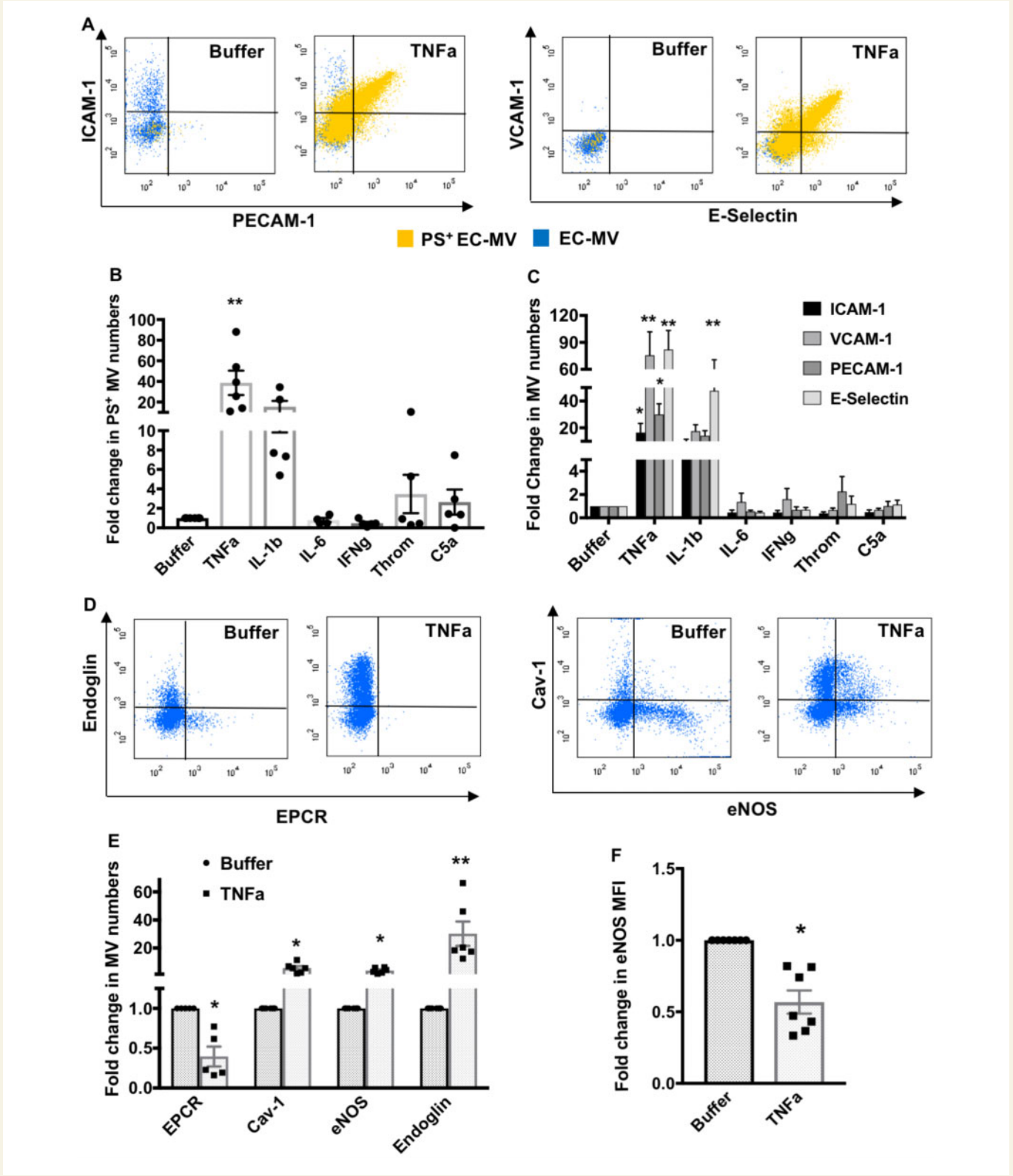

Figure 2 *In vitro* inflammatory stimulation alters endothelial MV numbers and cargos. (*A*) Representative flow cytometry dot plots demonstrate increased ICAM-1, PECAM-1, VCAM-1, E-selectin, and PS positive MVs generated from HUVECs treated with TNFα. (*B*) PS^+ EC-MV generation is significantly increased by TNFα treatment ($n = 5–6$ experiments). (*C*) TNFα significantly increased ICAM-1^+, VCAM-1^+, PECAM-1^+, and E-selectin$^+$ EC-MV generation, while IL-1β only significantly increased E-selectin$^+$ EC-MV generation from HUVECs ($n = 5–10$ experiments). $^{**}P < 0.01$ between buffer and individual inflammatory mediators by one-way ANOVA analysis and Dunnett's multiple comparison tests. (*D* and *E*) Flow cytometry analyses of TNFα-induced EC-MVs containing EPCR$^+$, Cav-1^+, eNOS$^+$, and endoglin$^+$ cargos. $^*P < 0.05$, $^{**}P < 0.01$ between buffer and TNFα by Student's *t*-test, $n = 5–6$ experiments. (*F*) eNOS expression (median fluorescence intensity) is significantly reduced in EC-MVs induced by TNFα. $^*P < 0.05$ by Student's *t*-test, $n = 7$ experiments. All data are shown as mean ± SEM.

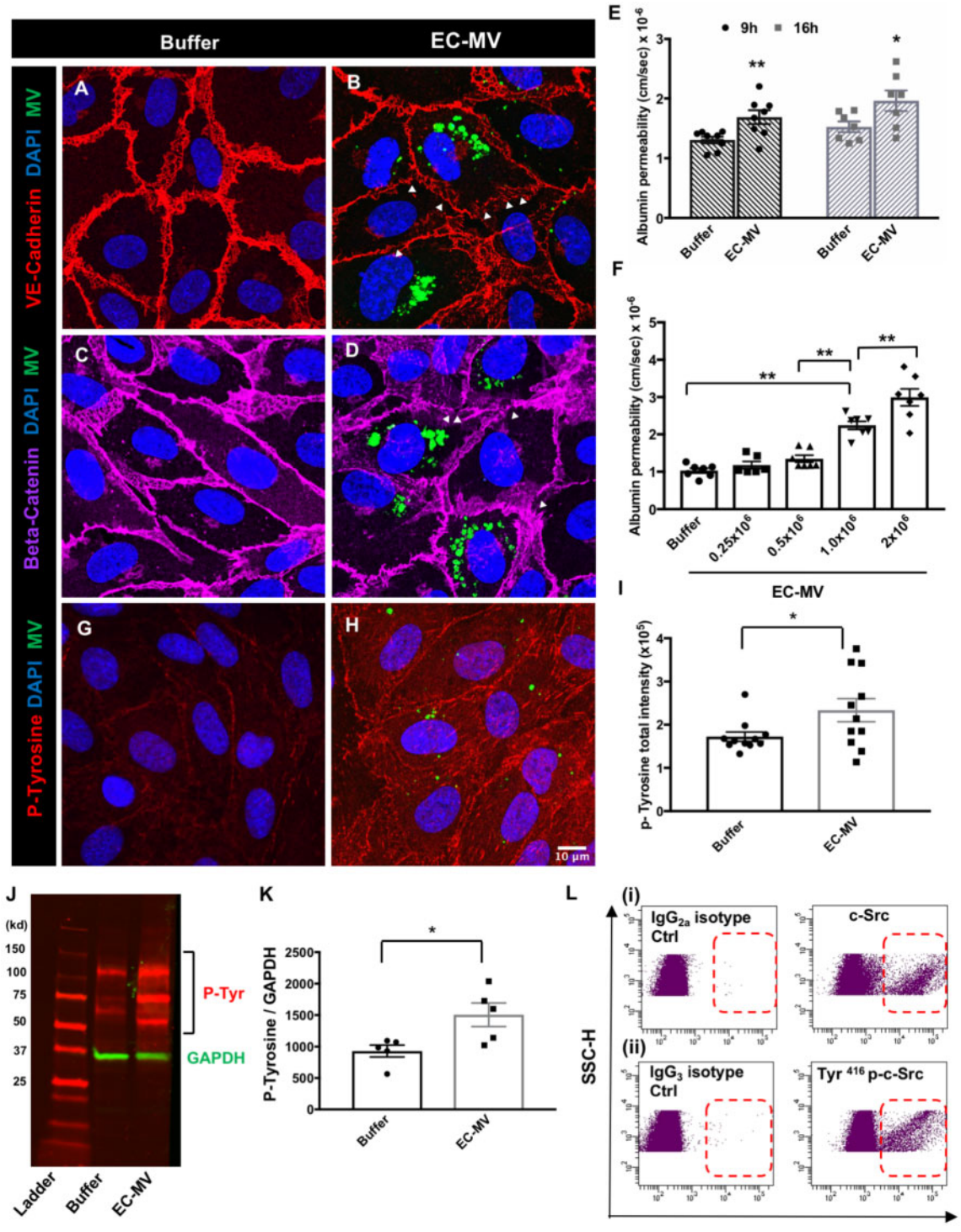

Figure 3 EC-MVs increase endothelial permeability and induce phosphorylation of proteins in recipient cells. (*A–D*) Representative confocal images showing discontinuous adherens junctions in HUVEC monolayers after EC-MV treatment. VE-cadherin (*A* and *B*) staining in buffer-treated and MV-treated ECs; (*C* and *D*) beta-catenin staining in HUVECs with and without EC-MVs (green dots indicate MVs, arrowheads point to discontinuous junction lining). (*E*) Albumin permeability through endothelial monolayers is increased after treatment with EC-MVs at 9 and 16 h. $^{*}P < 0.05$, $^{**}P < 0.01$ between buffer and EC-MV at 9 h and 16 h, respectively by Student's *t*-test, $n = 7–8$ experiments. (*F*) Albumin permeability through endothelial monolayers is increased after treatment with increasing concentration of EC-MVs. $^{**}P < 0.01$ by one-way ANOVA with Tukey's multiple comparison tests, $n = 6–7$ experiments. (*G–I*) Representative confocal images showing phospho-tyrosine level is remarkably increased after EC-MV treatment. Scale bar = 10µm and applies to all images. $^{*}P < 0.05$ by Student's *t*-test, $n = 11$ different confocal z stacks from multiple slides. (*J* and *K*) Western blot analysis showing phospho-tyrosine level is significantly increased after EC-MV treatment. $^{*}P < 0.05$ between control and EC-MV treated cells by Student's *t*-test, $n = 5$ lysates. All data are shown as mean ± SEM. (*L*) Representative flow cytometry dot plots show the presence of c-Src kinase and Tyr^{416} phosphorylated c-Src on EC-MVs.

permeability, which FITC-albumin permeability was increased in EC-MV treated endothelial monolayers at 9 and 16 h (*Figure 3E*). EC-MV increased EC monolayer permeability to albumin in a concentration-related manner (*Figure 3F*).

3.4 EC-MVs express c-Src and induce protein phosphorylation in recipient cells

Since barrier integrity is modulated by multiple intracellular signalling pathways involving phosphorylation of junction and cytoplasmic proteins, we investigated whether EC-MV targeting can cause phosphorylation of tyrosine residues of proteins in ECs. EC-MVs when added to HUVECs-induced tyrosine phosphorylation of membrane and cytosolic proteins (*Figure 3G–I*). The imaging data was supported by western blotting using antibodies against tyrosine phosphorylated proteins (*Figure 3J* and *K*). Since tyrosine phosphorylation of junction proteins are implicated in the pathogenesis of barrier disruption, we proceeded to examine whether EC-MVs contribute to this process by delivering cargos that promote tyrosine phosphorylation, such as the Src family of tyrosine kinases. Indeed, EC-MVs expressed a high level of c-Src (*Figure 3L(i)*) which is phosphorylated at Tyr^{416}. As tyrosine phosphorylation at this site is a commonly accepted indicator of Src activation, the data supports that c-Src in EC-MVs is activated (*Figure 3L(ii)*).

3.5 EC-MVs promote stress fibre formation, MLC and VE-cadherin phosphorylation

Endothelial paracellular permeability is dynamically regulated by cytoskeletal reorganization and via post-translational modifications (e.g. phosphorylation) of endothelial junction and intracellular molecules. We investigated the changes in the cytoskeleton of endothelial cells after adding EC-MVs. Our findings demonstrated that EC-MVs increased F-actin stress fibres (*Figure 4A–C*). Cortactin, an actin-binding protein, was increased by EC-MVs and exhibited more centralized localization as opposed to membrane localization (*Figure 4D–F*). In addition, EC-MVs caused myosin light chain (MLC2) phosphorylation (*Figure 4G* and *H*) at Thr^{18}/Ser^{19}, where phosphorylated MLC2 was colocalized with F-actin stress fibres (*Figure 4H* and *I*), suggestive of actomyosin contractile cytoskeleton reorganization. Three-dimensional reconstruction revealed that some MVs were internalized into the endothelial cytosol, while some bound to the cell membrane (*Figure 4I*). Such an interaction increased Tyr^{658} p-VE-Cadherin fluorescence intensity in target cells (*Figure 4J* and *K*). Consistent with these imaging results, western blotting confirmed the phosphorylation of MLC2 and VE-cadherin (*Figure 4L* and *M*). Treatment with 1 μM PP1, a Src inhibitor, was able to reduce VE-cadherin/beta-catenin dissociation at cell–cell junctions, stress fibre formation, VE-Cadherin, and MLC2 phosphorylation. It also reduced EC-MV-induced endothelial barrier dysfunction (Supplementary material online, *Figure S1*).

3.6 EC-MVs derived from c-Src deficient cells cause less stress fibre formation, protein phosphorylation, and albumin transendothelial flux

We harvested EC-MVs from endothelial cells with c-Src knockdown (KD) via siRNA gene silencing (scrambled siRNA as control) (*Figure 5A* and *B*). Compared to the controls, c-Src KD EC-MVs exerted an attenuated effect on albumin hyperpermeability in endothelial monolayers (*Figure 5C*). At the subcellular level, c-Src KD EC-MVs caused a significantly reduced effect on stress fibre formation (*Figure 5D–F*), cortactin level and subcellular distribution (*Figure 5G–I*), MLC2 phosphorylation (*Figure 5J–L*, *O*), or VE-cadherin phosphorylation at Tyr^{658} (*Figure 5L–O*).

3.7 EC-MVs increase surface expression of adhesion molecules on endothelial cells and cause activation of neutrophils

Flow cytometry analysis of live HUVECs revealed an increased expression of ICAM-1 and VCAM-1 after treatment with EC-MVs (*Figure 6A* and *B*). As neutrophil activation is an indicator of acute inflammation, we investigated the effects of EC-MVs on neutrophil activities. EC-MVs were added to human blood followed by flow cytometry analysis of neutrophil surface molecules. The results showed that CD11b on the neutrophil surface was up-regulated after EC-MV treatment (*Figure 6C* and *D*). In cultured endothelial monolayers treated with EC-MVs, increased neutrophil adhesion was observed (*Figure 6E* and *F*). In separate experiments, isolated neutrophils were seeded on coverslips and their response to EC-MVs was examined. EC-MVs were capable of promoting the release of neutrophil extracellular traps (NETs) containing citrullinated histones and myeloperoxidase (*Figure 6G*). Additionally, EC-MVs-induced NETosis in a concentration-related manner (Supplementary material online, *Figure S2A*). In contrast to the MV-induced endothelial barrier response, MV-induced NETosis and CD11b up-regulation were not dependent on c-Src signalling (*Figure 6H* and Supplementary material online, *Figure S2B–C*).

Hence, EC-MVs produced during inflammation alter endothelial barrier function via a direct effect on protein phosphorylation and/or indirect effects on neutrophil adhesion and releasing NETs, which in turn exacerbate barrier injury (*Figure 7*).

4. Discussion

The biomarker role of endothelium-derived MVs in diagnosis/prognosis of cardiovascular diseases has been well-recognized.[11,17,26,27] Recent studies suggest that they are also involved in the pathogenesis of chronic inflammatory diseases.[28] However, their specific contributions to leucocyte-endothelium interactions and barrier regulation during acute inflammation remain unclear. In this study, we demonstrate that (i) sepsis and inflammatory agents stimulate EC-MV production and release into the circulation; (ii) the total level, size distribution, and molecular properties of MVs are heterogeneous in response to different stimuli; (iii) EC-MVs directly interact with endothelial cells causing junction and cytoskeleton protein phosphorylation, contractile cytoskeleton reorganization and adherens junction dissociation, functionally measured as increased albumin permeability; (iv) EC-MVs cause barrier dysfunction by delivering cargos containing c-Src, whereas MVs from endothelial cells deficient of Src display minimal effects on barrier morphology and function; and (v) EC-MVs promote neutrophil-endothelium adhesion and induce NET production, both are known to contribute to endothelial barrier dysfunction. These findings provide novel insights into the roles and mechanisms by which EC-MVs contribute to inflammatory injury.

MVs are formed through outward blebbing of the plasma membrane, which results in exposure of phosphatidylserine on the MV surface.[29] These MVs carry a diverse cargo that can be transferred to other cells to regulate multiple processes in autocrine or paracrine manners.[29] The quantity and cargo contents of MVs vary depending on the origin and state of parent cells. We detected increased MVs of endothelial origin in

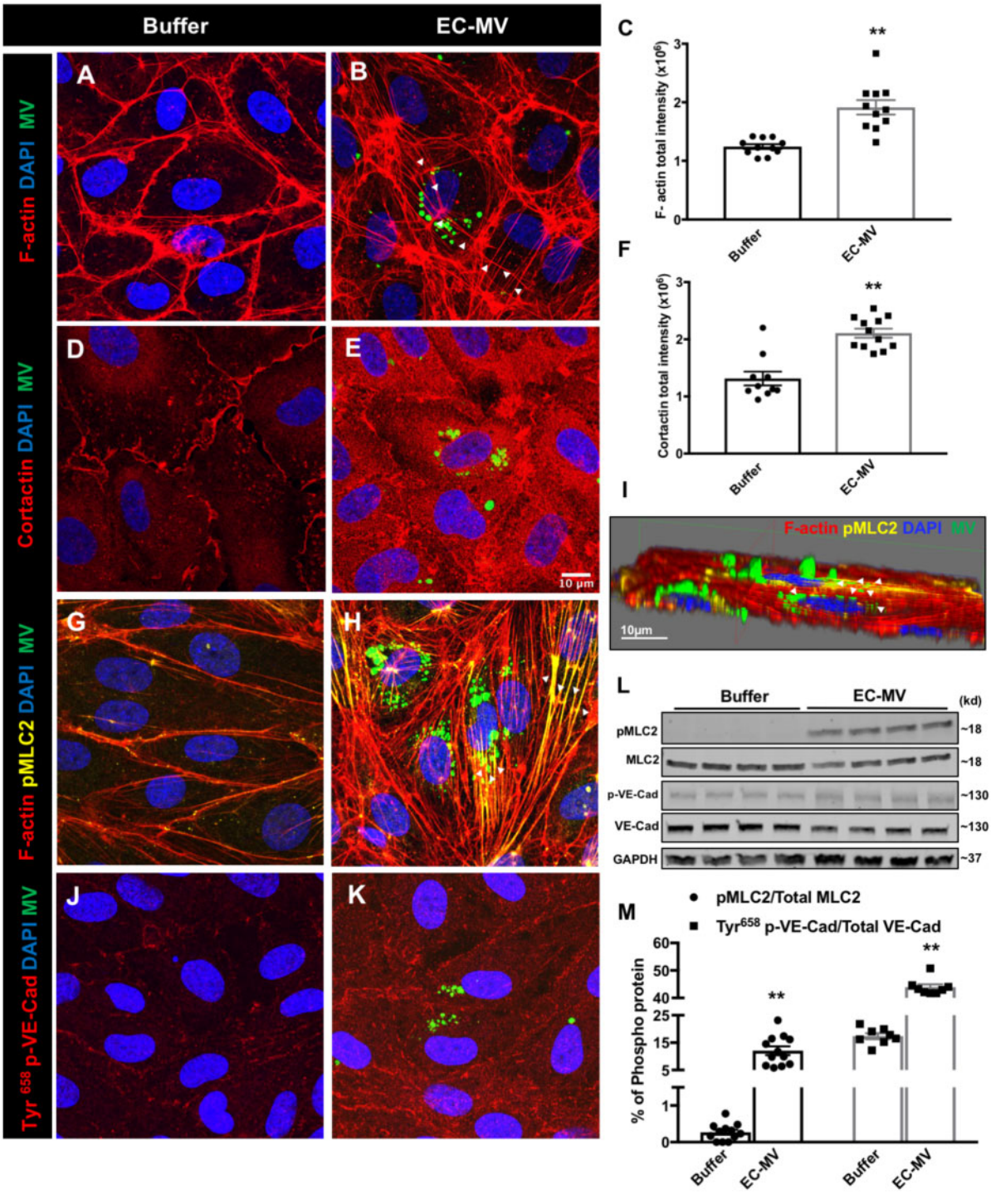

Figure 4 EC-MVs promote stress fibre formation, MLC, and VE-cadherin phosphorylation. (*A–C*) Representative confocal microscopy images and z stack analysis showing increased F-actin stress fibres (arrowheads) in ECs after EC-MV interaction. (*D–F*) The actin-binding protein cortactin is increased and redistributes from the cell periphery to more centralized intracellular locations after EC-MV treatment. Scale bar corresponds to 10µm and applies to all images.**$P < 0.01$ between buffer and EC-MV treated cells by Student's *t*-test, $n = 10–12$ different confocal z stacks from multiple slides. (*G* and *H*) Representative confocal microscopy images showing EC-MV interaction with ECs increase pMLC2 (Thr18/Ser19) which co-stains with F actin (arrowheads). (*I*) A three-dimensional reconstruction of *Panel H* reveal MVs fused to the cell membrane as well as inside the cell (arrowheads) at the same focal plane with F-actin stress fibres and pMLC2. (*J* and *K*) Representative confocal microscopy images showing EC-MV interaction increases Tyr^{658} p-VE-Cadherin compared to control cells. (*L* and *M*) Representative western blot images and analysis showing increased percentage of phosphorylated MLC2 and VE-cadherin after EC-MV treatment. All data are shown as mean ± SEM. **$P < 0.01$ by Student's *t*-test, $n = 8$ lysates.

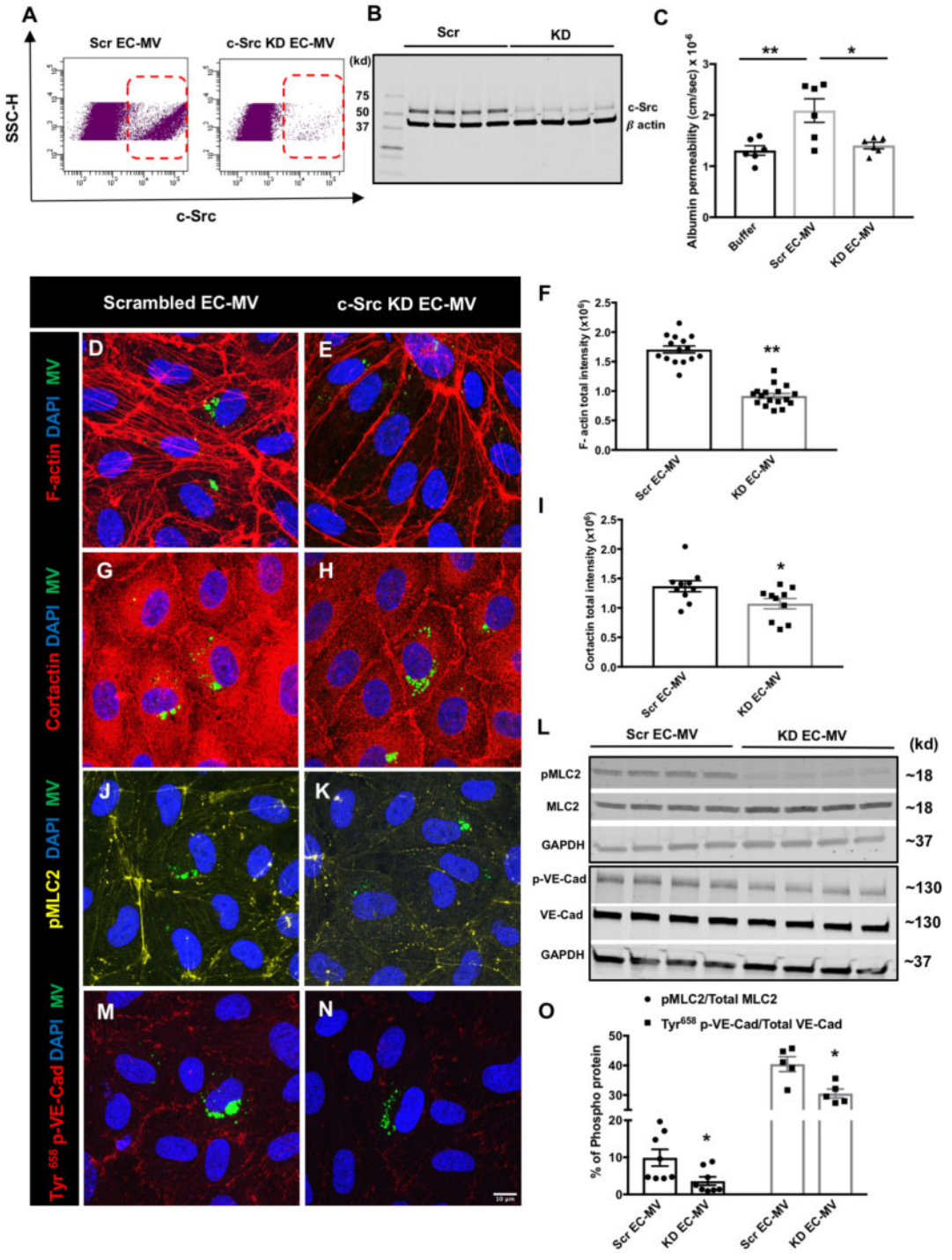

Figure 5 EC-MVs deficient in c-Src have reduced effects on albumin flux, stress fibre formation, MLC, and VE-cadherin phosphorylation. (*A*) EC-MVs derived from c-Src knockdown HUVECs display negligible c-Src compared to those from scrambled siRNA-treated cells, confirming the efficiency of c-Src knockdown. (*B*) Western blot image showing knockdown of intracellular c-Src in ECs after transfection with c-Src siRNA. (*C*) Albumin permeability through endothelial monolayers is increased at 16 h after treatment with scrambled EC-MVs but not by c-Src deficient EC-MVs. $^{*}P < 0.05$, $^{**}P < 0.01$ by one-way ANOVA with Tukey's multiple comparison tests, $n = 6$ experiments. (*D–F*) Confocal microscopy z stack analysis comparing F-actin levels in endothelial monolayers treated with scrambled vs. Src-deficient EC-MVs. (*G–I*) Comparison of cortactin levels from confocal z stacks in endothelial cells treated with scrambled vs. Src-deficient EC-MVs. $^{*}P < 0.05$, $^{**}P < 0.01$ by Student's *t*-test, $n = 10–18$ different confocal z stacks from multiple slides. Representative confocal images showing increased phospho-MLC levels (*J* and *K*) and Tyr^{658} p-VE-Cadherin levels (*M* and *N*) in endothelial cells treated with scrambled vs. Src-deficient EC-MVs. Scale bar corresponds to 10μm and applies to all images. (*L*, *O*) Western blot images and analysis showing increased percentage of pMLC2 and Tyr^{658} p-VE-Cadherin in endothelial cells treated with scrambled vs. Src-deficient EC-MVs. Data are shown as mean ± SEM. $^{**}P < 0.01$ by Student's *t*-test, $n = 5–8$ lysates.

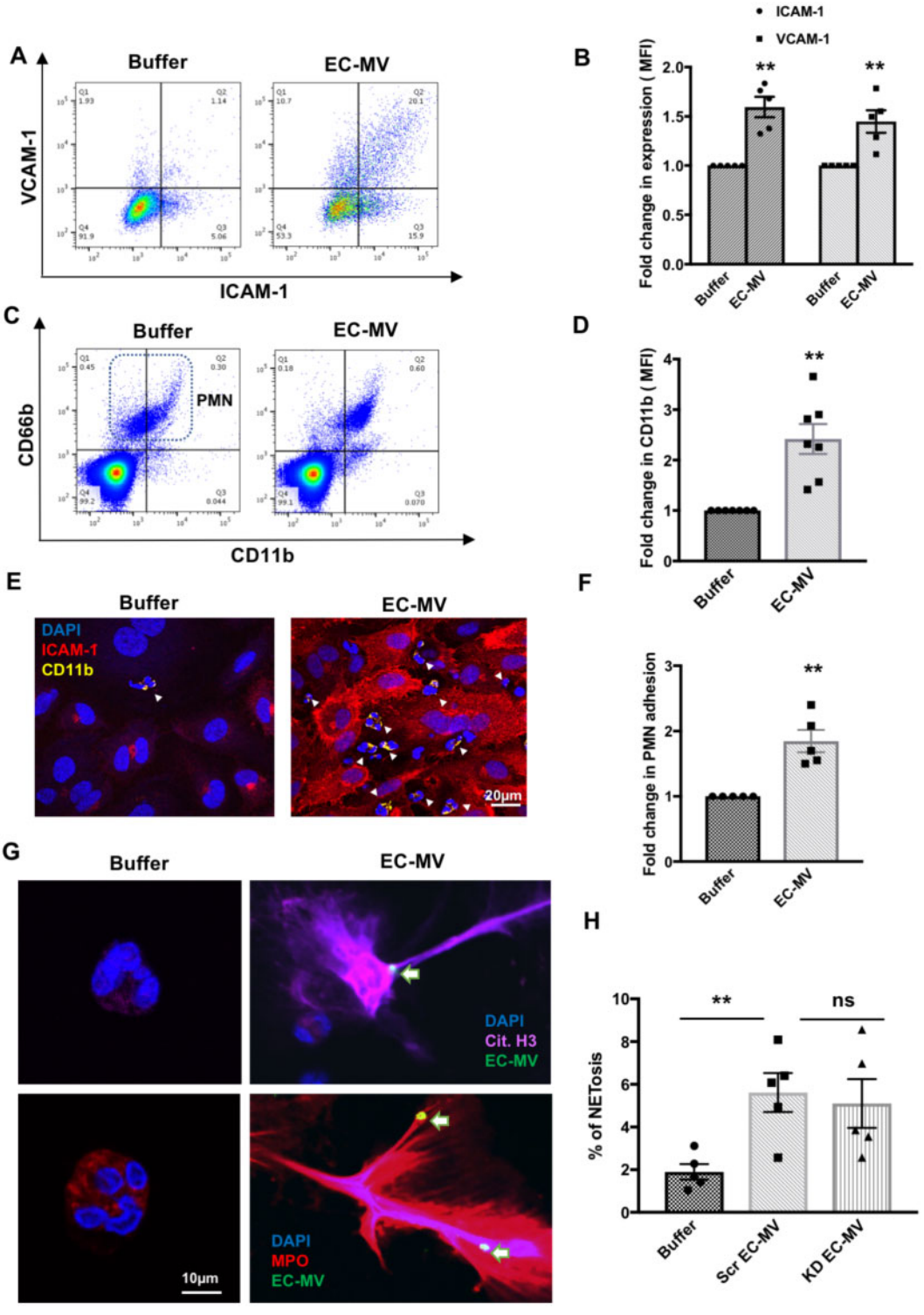

Figure 6 EC-MVs cause activation of neutrophils and endothelial cells. (*A* and *B*) Flow cytometry analyses show significantly increased ICAM-1 and VCAM-1 expression on HUVECs after treatment with EC-MVs for 4 h. $^{**}P < 0.01$ between buffer and EC-MV by Student's *t*-test, $n = 5$ experiments. (*C* and *D*) Whole blood flow cytometry analyses show increased levels of CD11b on neutrophil surface after treatment with EC-MVs for 2 h. CD66b was used as a marker of neutrophils. $^{**}P < 0.01$ by Student's *t*-test, $n = 7$ experiments. (*E* and *F*) Representative confocal images and cell adhesion assay showing increased EC-PMN adhesion after EC-MV treatment. $^{**}P < 0.01$ by Student's *t*-test, $n = 5$ experiments. Arrowheads indicate adherent neutrophils. Scale bar = 20 μm. (*G*) EC-MV interaction with neutrophils induce NET formation. (Left panel) Unstimulated neutrophil and (right panel) neutrophils stimulated by EC-MVs showing NET formation, arrow points to MVs. Scale bar = 10 μm. (*H*) Increased percentage of neutrophils undergoing NETosis following treatment with EC-MVs. There was no statistical difference in NET formation between c-Src KD EC-MVs and scrambled EC-MVs. $^{**}P < 0.01$, ns = not significant by one-way ANOVA analysis, $n = 5$ experiments. All data are shown as mean ± SEM.

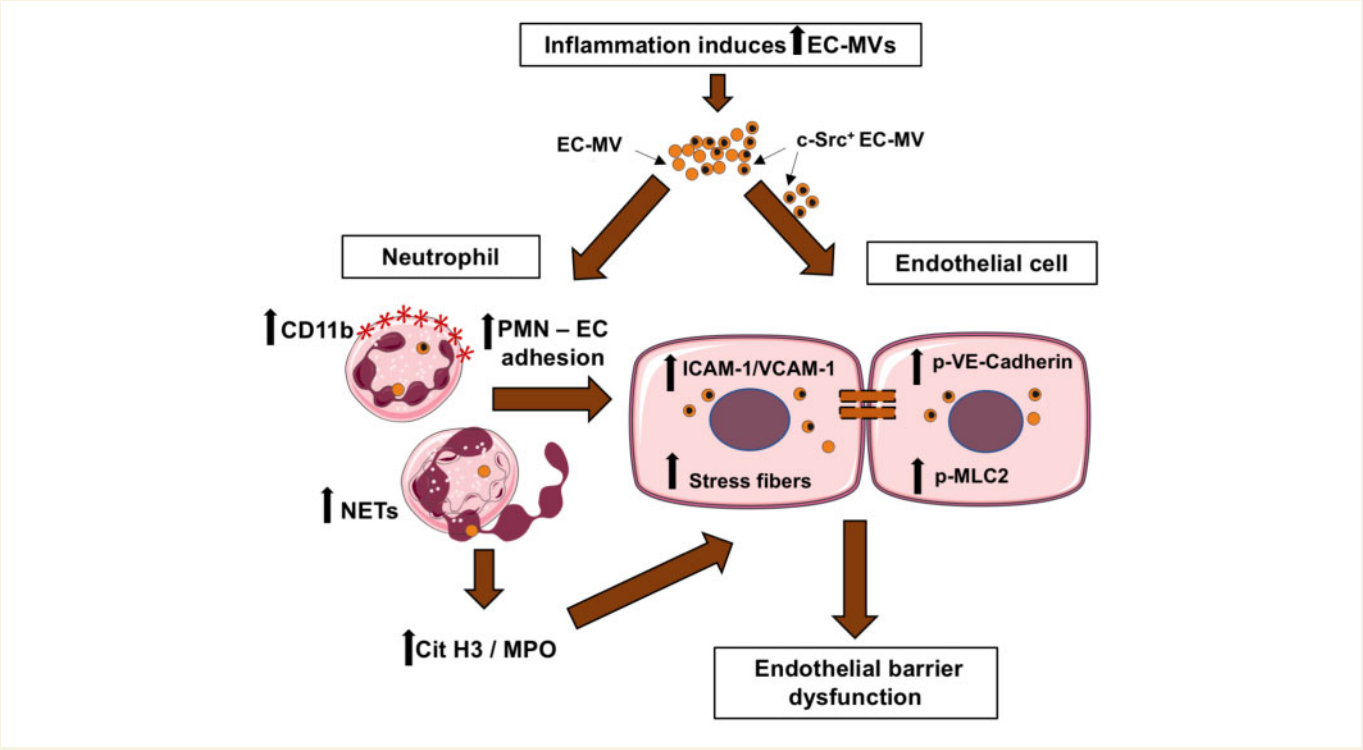

Figure 7 Schematic diagram summarizing the effects of inflammation induced EC-MVs on endothelial and neutrophil activation. Inflammatory injury increases the production of endothelial microvesicles. Src^+ EC-MVs disrupt endothelial barrier integrity by increasing acto-myosin contractility through stress fibre formation and increased phosphorylation of MLCK. Src^+ EC-MVs increase tyrosine phosphorylation of VE-cadherin and increase albumin permeability through endothelial monolayers. EC-MVs also contribute to vascular injury indirectly by increasing adhesion molecules on ECs and neutrophils to enhance PMN-EC adhesion and by promoting NETosis with release of citrullinated histone H3 and myeloperoxidase. Images of cells were obtained from Smart Servier Medical Art (https://smart.servier.com).

the plasma of sepsis mice. We also found that different inflammatory agents (e.g. cytokines, thrombin) induce EC-MV production in different patterns. For example, EC-MVs produced during TNFα stimulation displayed increased PS expression and reduced EPCR, indicative of their pro-inflammatory/coagulant nature.[30,31] In addition, circulating MVs have been shown to carry functional eNOS protein that can generate nitric oxide (NO),[32,33] a known inhibitor of platelet aggregation.[34] Caveolin-1 is a negative regulator of eNOS activity.[35] Endoglin inhibits TGF-β1 binding to its receptors and impairs eNOS activity.[36] Thus, MVs with decreased eNOS expression coupled with increased Cav-1 and endoglin may contribute to impaired vasoactivity and thrombotic injury during sepsis.

The current study centres on the endothelial barrier effects of EC-MVs. Endothelial junction dissociation coupled with contractile cytoskeleton reorganization is a hallmark of paracellular barrier dysfunction during inflammation. Contractile cytoskeleton consists of filamentous (F) actin and myosin; their cross-bridge movement is triggered by myosin light chain phosphorylation (Thr^{18}/Ser^{19}) mediated by myosin light chain kinase, whose activity is promoted by tyrosine phosphorylation. Non-muscle myosin light chain kinase contains multiple sites of tyrosine that can be phosphorylated by tyrosine kinases.[37] In an initial screening test, we detected the presence of several tyrosine kinases in EC-MVs, including the Src-family (c-Src, Fyn) and focal adhesion kinase. We selected c-Src for study because it is known to be a major signalling molecule in permeability regulation, and because it is one of the most important mediator in MLCK-dependent cytoskeleton contractile response.[38] Additionally, cortactin, a cytoskeletal protein associated with MLCK[39] is capable of promoting actin polymerization. In quiescent endothelial cells, cortactin is usually present in the cell periphery, contributing to the maintenance of cortical actin rim that stabilizes cell spherical shape and junction adhesion.[40] Upon MV stimulation, cortactin moved from cell periphery to a more centralized cytosolic location where it promoted actin polymerization to form stress fibres. Cortactin is a known substrate for Src kinases.[40–42] In addition, c-Src has also been implicated in VE-cadherin phosphorylation which causes adherens junction dissociation or disassembly.[43,44] Our data that Src^+ EC-MVs, but not Src^- EC-MVs, induce stress fibre formation and junction discontinuity further support its important role in the paracellular permeability response to MVs. Based on these results, we propose that EC-MVs produced during sepsis or inflammatory stimulation can directly interact with the endothelium and cause barrier dysfunction by delivering pro-inflammatory cargos containing c-Src, which promotes endothelial contractile stress and junction dissociation via protein phosphorylation.

In addition to their direct effects on endothelial cytoskeleton-junction, EC-MVs also promote neutrophil-endothelium interactions, evidenced by increased neutrophil adherence to endothelium, as well as increased expression of adhesion molecules on both neutrophils (CD11b) and endothelial surface (ICAM-1, VCAM-1). These membrane-bound molecules are known to mediate neutrophil adhesion and transendothelial migration,[45] which are often coupled with barrier opening. Interestingly, we detected neutrophil extracellular traps produced by neutrophils upon stimulation with EC-MVs, indicating their ability to alter neutrophil

activities, including NETosis, a programmed cell death process where neutrophils release DNA decorated with citrullinated histones and granular enzymes such as myeloperoxidase and elastase.[46] We have recently identified citrullinated histone 3 as a primary protein component of NETs that is capable of increasing microvascular permeability by causing endothelial paracellular leakage.[47] The role of myeloperoxidase in inflammation has been well-documented with many studies reporting its involvement in endothelial permeability both *in vivo* and *in vitro*.[48] Therefore, we postulate that EC-MVs produced during inflammation can alter endothelial junction integrity via a direct effect on protein phosphorylation and/or indirect effects on neutrophil adhesion and releasing NETs, which in turn exacerbate barrier injury. While the phosphorylation pathway is mediated by Src-dependent signalling transduced via Src-laden cargo, the MV-induced neutrophil activity in NETosis does not seem to require Src.

Although our mechanistic hypothesis is focused on the EC origin of MV production and their effects on endothelial barrier dysfunction via the Src-pathway, we recognize the various cell origins of MVs and their heterogeneous responses to different stimuli or disease conditions. Further investigation is warranted to characterize additional MV cargo contents including other protein kinases, as well as their cell-specific mechanisms of generation and action under particular inflammatory conditions. Within this context, HUVECs used in the current study has limitations as they do not represent barrier cells from adult tissues. In our future studies, we plan to use microvascular endothelial cells from adult human or animal organs/tissues that are more physiologically relevant. We also plan to carry out a more in-depth molecular analysis of the mechanisms by which MVs target endothelial cells. Based on the current data, it is plausible that MVs interact with target cells via multiple means, including by releasing soluble cargo contents, binding to cell membrane or surface receptors, and internalization into cytosol to interact with intracellular molecules. Additionally, in the *in vitro* experiments, MVs were added to endothelial cells at a ratio of approximately 50:1 (MV:EC). While this concentration was selected based on previous literature and the current dose-response data (*Figure 3*), it may not fully resemble the *in vivo* conditions of sepsis or other cardiovascular pathologies, especially those with localized inflammatory injury or lesions. Thus, further studies are required to evaluate the *in vivo* response of EC-MV production and their effects in specific models of cardiovascular disease.

In summary, we demonstrate that endothelial production of MVs is increased during sepsis and cytokine stimulation. EC-MVs directly interact with endothelial cells causing a barrier response characterized by contractile cytoskeleton reorganization and adherens junction dissociation; these cellular responses were coupled with protein phosphorylation mediated by MV cargos containing c-Src. In addition, EC-MVs promote neutrophil-endothelium adhesion and stimulate NETosis via a c-Src independent pathway.

Supplementary material

Supplementary material is available at *Cardiovascular Research* online.

Authors' contribution

V.C. performed, analysed, and interpreted most of the experiments. X.Y. participated in animal studies. B.J.C. assisted with confocal imaging analyses. Y.M., J.E.M., and M.W. participated in experimental design and data interpretation. S.Y.Y. initiated, directed, and sponsored the work throughout all levels of development. All the authors discussed the results and approved the manuscript.

Acknowledgements

We thank Jonathan Overstreet and Alexandria Creasy for their technical assistance.

Conflict of interest: none declared.

Funding

This work was supported by the National Institutes of Health [HL126646, HL070752, and GM097270]. The IRB-approved work was supported by the University of South Florida research startup funds.

References

1. Yuan SY, Shen Q, Rigor RR, Wu MH. Neutrophil transmigration, focal adhesion kinase and endothelial barrier function. *Microvasc Res* 2012;**83**:82–88.
2. Yuan SY, Rigor RR. *Regulation of Endothelial Barrier Function*. San Rafael, CA: Morgan and Claypool Life Sciences; 2010.
3. Shen Q, Wu MH, Yuan SY. Endothelial contractile cytoskeleton and microvascular permeability. *Cell Health Cytoskelet* 2009;**2009**:43–50.
4. Raposo G, Stoorvogel W. Extracellular vesicles: exosomes, microvesicles, and friends. *J Cell Biol* 2013;**200**:373–383.
5. Lo Cicero A, Stahl PD, Raposo G. Extracellular vesicles shuffling intercellular messages: for good or for bad. *Curr Opin Cell Biol* 2015;**35**:69–77.
6. Schiro A, Wilkinson FL, Weston R, Smyth JV, Serracino-Inglott F, Alexander MY. Endothelial microparticles as conveyors of information in atherosclerotic disease. *Atherosclerosis* 2014;**234**:295–302.
7. Tushuizen ME, Diamant M, Sturk A, Nieuwland R. Cell-derived microparticles in the pathogenesis of cardiovascular disease: friend or foe? *Arterioscler Thromb Vasc Biol* 2011;**31**:4–9.
8. VanWijk MJ, VanBavel E, Sturk A, Nieuwland R. Microparticles in cardiovascular diseases. *Cardiovasc Res* 2003;**59**:277–287.
9. VanWijk MJ, Nieuwland R, Boer K, van der Post JA, VanBavel E, Sturk A. Microparticle subpopulations are increased in preeclampsia: possible involvement in vascular dysfunction? *Am J Obstet Gynecol* 2002;**187**:450–456.
10. Sinning JM, Losch J, Walenta K, Bohm M, Nickenig G, Werner N. Circulating CD31+/Annexin V+ microparticles correlate with cardiovascular outcomes. *Eur Heart J* 2011;**32**:2034–2041.
11. Amabile N, Heiss C, Real WM, Minasi P, McGlothlin D, Rame EJ, Grossman W, De Marco T, Yeghiazarians Y. Circulating endothelial microparticle levels predict hemodynamic severity of pulmonary hypertension. *Am J Respir Crit Care Med* 2008;**177**:1268–1275.
12. Heloire F, Weill B, Weber S, Batteux F. Aggregates of endothelial microparticles and platelets circulate in peripheral blood. Variations during stable coronary disease and acute myocardial infarction. *Thromb Res* 2003;**110**:173–180.
13. Chirinos JA, Heresi GA, Velasquez H, Jy W, Jimenez JJ, Ahn E, Horstman LL, Soriano AO, Zambrano JP, Ahn YS. Elevation of endothelial microparticles, platelets, and leukocyte activation in patients with venous thromboembolism. *J Am Coll Cardiol* 2005;**45**:1467–1471.
14. Brodsky SV, Zhang F, Nasjletti A, Goligorsky MS. Endothelium-derived microparticles impair endothelial function *in vitro*. *Am J Physiol Heart Circ Physiol* 2004;**286**:H1910–H1915.
15. Vanwijk MJ, Svedas E, Boer K, Nieuwland R, Vanbavel E, Kublickiene KR. Isolated microparticles, but not whole plasma, from women with preeclampsia impair endothelium-dependent relaxation in isolated myometrial arteries from healthy pregnant women. *Am J Obstet Gynecol* 2002;**187**:1686–1693.
16. Martin S, Tesse A, Hugel B, Martínez MC, Morel O, Freyssinet J-M, Andriantsitohaina R. Shed membrane particles from T lymphocytes impair endothelial function and regulate endothelial protein expression. *Circulation* 2004;**109**:1653–1659.
17. Boulanger CM, Scoazec A, Ebrahimian T, Henry P, Mathieu E, Tedgui A, Mallat Z. Circulating microparticles from patients with myocardial infarction cause endothelial dysfunction. *Circulation* 2001;**104**:2649–2652.
18. Delabranche X, Boisrame-Helms J, Asfar P, Berger A, Mootien Y, Lavigne T, Grunebaum L, Lanza F, Gachet C, Freyssinet JM, Toti F, Meziani F. Microparticles are new biomarkers of septic shock-induced disseminated intravascular coagulopathy. *Intensive Care Med* 2013;**39**:1695–1703.
19. Chaudhry H, Zhou J, Zhong Y, Ali MM, McGuire F, Nagarkatti PS, Nagarkatti M. Role of cytokines as a double-edged sword in sepsis. *In Vivo* 2013;**27**:669–684.
20. Schulte W, Bernhagen J, Bucala R. Cytokines in sepsis: potent immunoregulators and potential therapeutic targets—an updated view. *Mediators Inflamm* 2013;**2013**:1.

21. Guo RF, Ward PA. C5a, a therapeutic target in sepsis. *Recent Pat Antiinfect Drug Discov* 2006;**1**:57–65.
22. Ward PA. The dark side of C5a in sepsis. *Nat Rev Immunol* 2004;**4**:133–142.
23. Petros S, Kliem P, Siegemund T, Siegemund R. Thrombin generation in severe sepsis. *Thromb Res* 2012;**129**:797–800.
24. Yang X, Meegan JE, Jannaway M, Coleman DC, Yuan SY. A disintegrin and metalloproteinase 15-mediated glycocalyx shedding contributes to vascular leakage during inflammation. *Cardiovasc Res* 2018;**114**:1752–1763.
25. Sabatier F, Roux V, Anfosso F, Camoin L, Sampol J, Dignat-George F. Interaction of endothelial microparticles with monocytic cells *in vitro* induces tissue factor-dependent procoagulant activity. *Blood* 2002;**99**:3962–3970.
26. Amabile N, Guerin AP, Leroyer A, Mallat Z, Nguyen C, Boddaert J, London GM, Tedgui A, Boulanger CM. Circulating endothelial microparticles are associated with vascular dysfunction in patients with end-stage renal failure. *J Am Soc Nephrol* 2005;**16**:3381–3388.
27. Boulanger CM, Amabile N, Tedgui A. Circulating microparticles: a potential prognostic marker for atherosclerotic vascular disease. *Hypertension* 2006;**48**:180–186.
28. Koga H, Sugiyama S, Kugiyama K, Watanabe K, Fukushima H, Tanaka T, Sakamoto T, Yoshimura M, Jinnouchi H, Ogawa H. Elevated levels of VE-cadherin-positive endothelial microparticles in patients with type 2 diabetes mellitus and coronary artery disease. *J Am Coll Cardiol* 2005;**45**:1622–1630.
29. Dignat-George F, Boulanger CM. The many faces of endothelial microparticles. *Arterioscler Thromb Vasc Biol* 2011;**31**:27–33.
30. Zhao L, Wu X, Si Y, Yao Z, Dong Z, Novakovic VA, Guo L, Tong D, Chen H, Bi Y, Kou J, Shi H, Tian Y, Hu S, Zhou J, Shi J. Increased blood cell phosphatidylserine exposure and circulating microparticles contribute to procoagulant activity after carotid artery stenting. *J Neurosurg* 2017;**127**:1041–1054.
31. Toltl LJ, Beaudin S, Liaw PC; Canadian Critical Care Translational Biology Group. Activated protein C up-regulates IL-10 and inhibits tissue factor in blood monocytes. *J Immunol* 2008;**181**:2165–2173.
32. Motta-Mejia C, Kandzija N, Zhang W, Mhlomi V, Cerdeira AS, Burdujan A, Tannetta D, Dragovic R, Sargent IL, Redman CW, Kishore U, Vatish M. Placental vesicles carry active endothelial nitric oxide synthase and their activity is reduced in preeclampsia. *Hypertension* 2017;**70**:372–381.
33. Horn P, Cortese-Krott MM, Amabile N, Hundsdorfer C, Kroncke KD, Kelm M, Heiss C. Circulating microparticles carry a functional endothelial nitric oxide synthase that is decreased in patients with endothelial dysfunction. *J Am Heart Assoc* 2012;**2**:e003764.
34. Wang GR, Zhu Y, Halushka PV, Lincoln TM, Mendelsohn ME. Mechanism of platelet inhibition by nitric oxide: *in vivo* phosphorylation of thromboxane receptor by cyclic GMP-dependent protein kinase. *Proc Natl Acad Sci USA* 1998;**95**:4888–4893.
35. Sowa G. Caveolae, caveolins, cavins, and endothelial cell function: new insights. *Front Physiol* 2012;**2**:120.
36. Venkatesha S, Toporsian M, Lam C, Hanai J, Mammoto T, Kim YM, Bdolah Y, Lim KH, Yuan HT, Libermann TA, Stillman IE, Roberts D, D'Amore PA, Epstein FH, Sellke FW, Romero R, Sukhatme VP, Letarte M, Karumanchi SA. Soluble endoglin contributes to the pathogenesis of preeclampsia. *Nat Med* 2006;**12**:642–649.
37. Birukov KG, Csortos C, Marzilli L, Dudek S, Ma SF, Bresnick AR, Verin AD, Cotter RJ, Garcia JG. Differential regulation of alternatively spliced endothelial cell myosin light chain kinase isoforms by p60(Src). *J Biol Chem* 2001;**276**:8567–8573.
38. Tinsley JH, Ustinova EE, Xu W, Yuan SY. Src-dependent, neutrophil-mediated vascular hyperpermeability and beta-catenin modification. *Am J Physiol Cell Physiol* 2002;**283**:C1745–C1751.
39. Dudek SM, Birukov KG, Zhan X, Garcia JG. Novel interaction of cortactin with endothelial cell myosin light chain kinase. *Biochem Biophys Res Commun* 2002;**298**:511–519.
40. Tehrani S, Tomasevic N, Weed S, Sakowicz R, Cooper JA. Src phosphorylation of cortactin enhances actin assembly. *Proc Natl Acad Sci USA* 2007;**104**:11933–11938.
41. Wu H, Reynolds AB, Kanner SB, Vines RR, Parsons JT. Identification and characterization of a novel cytoskeleton-associated pp60src substrate. *Mol Cell Biol* 1991;**11**:5113–5124.
42. Yang L, Kowalski JR, Yacono P, Bajmoczi M, Shaw SK, Froio RM, Golan DE, Thomas SM, Luscinskas FW. Endothelial cell cortactin coordinates intercellular adhesion molecule-1 clustering and actin cytoskeleton remodeling during polymorphonuclear leukocyte adhesion and transmigration. *J Immunol* 2006;**177**:6440–6449.
43. Dejana E, Orsenigo F, Lampugnani MG. The role of adherens junctions and VE-cadherin in the control of vascular permeability. *J Cell Sci* 2008;**121**:2115–2122.
44. Wessel F, Winderlich M, Holm M, Frye M, Rivera-Galdos R, Vockel M, Linnepe R, Ipe U, Stadtmann A, Zarbock A, Nottebaum AF, Vestweber D. Leukocyte extravasation and vascular permeability are each controlled *in vivo* by different tyrosine residues of VE-cadherin. *Nat Immunol* 2014;**15**:223–230.
45. Skubitz KM, Campbell KD, Skubitz AP. CD66a, CD66b, CD66c, and CD66d each independently stimulate neutrophils. *J Leukoc Biol* 1996;**60**:106–117.
46. Delgado-Rizo V, Martínez-Guzmán MA, Iñiguez-Gutierrez L, García-Orozco A, Alvarado-Navarro A, Fafutis-Morris M. Neutrophil extracellular traps and its implications in inflammation: an overview. *Front Immunol* 2017;**8**:81.
47. Meegan JE, Yang X, Beard RS Jr, Jannaway M, Chatterjee V, Taylor-Clark TE, Yuan SY. Citrullinated histone 3 causes endothelial barrier dysfunction. *Biochem Biophys Res Commun* 2018;**503**:1498–1502.
48. Ullen A, Singewald E, Konya V, Fauler G, Reicher H, Nusshold C, Hammer A, Kratky D, Heinemann A, Holzer P, Malle E, Sattler W. Myeloperoxidase-derived oxidants induce blood-brain barrier dysfunction *in vitro* and *in vivo*. *PLoS One* 2013;**8**:e64034.

Translational perspective

Circulating microvesicles derived from blood/vascular cells not only serve as serological markers of disease but also play a pathogenic role in vascular inflammation. In this study, we characterized the production and molecular signature of microparticles produced by endothelial cells under inflammatory conditions. We discovered that these vesicles carry Src-bearing cargo which interact with endothelial cells inducing cytoskeleton contractile stress and impaired VE-cadherin junction integrity. Additionally, endothelial-derived MVs are capable of stimulating neutrophil–endothelium adhesion and production of neutrophil extracellular traps containing citrullinated histones and myeloperoxidase. These novel findings have the potential to be translated into the development of diagnostic or therapeutic strategies to treat inflammatory disease.